Supporting Information

Expression of Interfacial Seebeck Coefficient through Grain Boundary Engineering with Multi-Layer Graphene Nanoplatelets

Yue Lin[ab], Maxwell Wood[a], Kazuki Imasato[a], Jimmy Jiahong Kuo[a], David Lam[a], Nooshin Mortazavi[cd], Tyler J. Slade[e], Stephen A. Hodge[f], Kai Xi[g], Mercouri G. Kanatzidis[e], David R. Clarke[c], Mark C. Hersam[a,e], G. Jeffrey Snyder[a]

[a]Department of Materials Science and Engineering, Northwestern University, Evanston, IL 60208, USA

[b]Cavendish Laboratory, University of Cambridge, Cambridge CB3 0HE, UK

[c]School of Engineering and Applied Sciences, Harvard University, Cambridge, MA 02138, USA

[d]Department of Materials Science and Engineering, Monash University, Clayton, VIC 3800, Australia

[e]Department of Chemistry, Northwestern University IL 60208, USA

[f]Versarien Plc., Cheltenham GL51 9LT, UK

[g]Department of Materials Science and Metallurgy, University of Cambridge, Cambridge CB3 0FS, UK

Table of Contents

54
55

S1: Disconnect between Theoretical and Experimental Approaches in Energy Filtering Literature

Various forms of the concept 'energy filtering' have been discussed in the field of thermoelectrics for well over 20 years. The idea of energy filtering is very attractive to this field because it has been proposed as a route to decouple a materials' Seebeck coefficient and conductivity, which potentially leads to high power factors. With such a long history one would reasonably expect to find some successful stories that have arisen out of energy filtering. Nevertheless, In practice there are few successful demonstrations of viable thermoelectric materials with improved *zT* via an energy filtering strategy.[1-3] A very recent review[3] stated "However, no significant improvement in PF has been achieved to date, since in practice the negative effects of energy barriers (electron scattering) pre-dominate, and their desirable positive effects, i.e., enhancing the electronic density of states (DOS), become insignificant.". A possible reason why previous studies have struggled is due to a disconnect between theoretical and experimental approaches. While most experimental studies of energy filtering acknowledge inhomogeneity in their material is important to create an energy filtering effect, most if not all theoretical analysis is done using a homogenous transport theory.

For most experimental studies of energy filtering, a homogeneous transport assumption[4, 5] (Matthiessen's rule for combining scattering mechanisms) is typically used. Matthiessen's rule is so thoroughly embedded into the thermoelectric community that many researchers are unaware they are making an assumption of homogeneous charge carrier concentration and additive probability of scattering events when

analyzing transport. Many of the papers[6, 7] acknowledge the inhomogeneity of their system and contend that this heterogeneity is important for the energy filtering effect. However, when they analyze their transport, they use homogenous transport equations based on Matthiessen's rule.

The commonly claimed characteristics of the energy filtering effect are an increase of the Seebeck coefficient without affecting the electrical conductivity and carrier density (decoupling of increase in Seebeck to changing carrier concentration/conductivity), which should result in a net increase in the maximum power factor[2, 3]. When reviewing a few key publications in 'energy filtering' field we asked the following list of step-by-step questions to investigate possible energy filtering effect claimed:

a. Does the material studied here show a change of the Seebeck coefficient that could not be explained by a change in the charge carrier concentration? (Could one argue that the energy filtering is observed?)

b. Does this decoupling result in a material with improved maximum power factor or improved electronic portion of the thermoelectric quality factor? (Is this effect beneficial?)

c. Is energy filtering the most likely explanation? If a more common effect is a possible explanation the answer should be 'No'.

d. Does the paper employ a heterogeneous transport model?

A summary of investigation in these papers was listed in **Table S1** followed by the in-depth discussion in each paper. From the result, we are able to conclude that most of the papers either lack the decoupling effect or don't show any benefit of energy

filtering. Furthermore, although most of the papers acknowledge the inhomogeneity of their systems and contend that this heterogeneity is important for the energy filtering effect, they used homogenous transport equations when they are analyzing their transport.

Table S1: Summary of 'energy filtering' papers investigated.

	Paper	Material	Decoupling Observed?	Benefit Observed?	Energy Filtering Most Likely Explanation?	Heterogenous Transport Model?
	This Work	Mg_3Sb_2/GNP	Yes	Yes	Yes	Yes
1	Nano Lett. 2012, 12, 4305[8]	$Bi_2Te_{2.7}Se_{0.3}$	No	N/A	No	No
2	J. Appl. Phys. 2014, 115, 053710[6]	β-Zn_4Sb_3	Yes	No	No	No
3	Nano Lett. 2011, 11, 2841[7]	Sb_2Te_3	Yes	No	No	No
4	Phys. Rev. B 2004, 70, 115334[9]	PbTe	Yes	No	Yes	No
5	Acta Mater. 2013, 61, 2087[10]	Ti(Co,Fe)Sb	Yes*	No	No	No
6	J. Appl. Phys. 2010, 108, 064322[11]	PbTe	No	N/A	No	No
7	Jpn. J. Appl. Phys. 2016, 55, 045802[12]	$Bi_{85}Sb_{15}$/ graphene	No	N/A	No	No

*Complicated mechanisms involved, see detailed discussion

A key aspect our work tries to highlight is an experimentally self-consistent heterogeneous transport model instead of homogenous transport assumption that previous studies have applied in analysis. This results in the concept of an interfacial Seebeck coefficient that has never been discussed previously. We show that with the presence of Kapitza resistance, the interfacial Seebeck coefficient can be easily defined in a self-consistent manner that cannot be easily explained otherwise. While using such

a heterogenous model might seem obvious in our work, it has never before been used previously.

We recognize that dispersing graphene in thermoelectric materials, even Mg_3Sb_2[13], has previously been tried. But, utilizing graphene as a grain boundary tool to delicately tune the energy filtering effect has never been well demonstrated. One of the key advances in our work is utilizing graphene to observe a long predicted but rarely seen effect, and then understanding this effect by modifying a foundational assumption in the standard transport model, rather than the simple idea of adding graphene to a thermoelectric material.

We believe our work will be of significant interest in the thermoelectric community and will inspire follow up studies in different material systems. However, the area of energy filtering in thermoelectric is currently met with skepticism due to conceptual confusion and poorly supported claims created from previous work. In order for this idea to receive the attention it deserves a clear experimental example and method to unequivocally show the effect.

Detailed Discussion in Individual Energy Filtering Papers

1 $Bi_2Te_{2.7}Se_{0.3}$ (Nano Lett. 2012, 12, 4305) [8]

a. Does the material studied here show a change of the Seebeck coefficient that could not be explained by a change in the charge carrier concentration? (Could one argue that the energy filtering is observed?)

Answer: No, the carrier concentration is not measured, and the trend in Seebeck and conductivity are what is expected for a change in charge carrier concentration except for one sample.

b. Does this decoupling result in a material with improved maximum power factor or improved electronic portion of the thermoelectric quality factor? (Is this effect beneficial?)

Answer: N/A. Decoupling effect is not observed.

c. Is electron filtering the most likely explanation?

Answer: No, the samples show varying degrees of texturing, with the best sample being the most textured. Bi_2Te_3 materials are known to have high anisotropy. It is very likely that the differences in transport properties witnessed are from differing degrees of texturing in the samples. Furthermore, this paper only measures samples in the in-plane direction, meaning the anisotropy has not been tested. Therefore, we cannot check to see the whole picture that texturing is having on this material's properties.

d. Does the paper employ a homogenous or inhomogeneous model for transport?

Answer: While this paper uses the 'interface driven energy filtering' in the title it gives no phenological explanation for energy filtering instead citing papers that are indirectly related and use a homogenous transport model.

2 β-Zn_4Sb_3 (J. Appl. Phys. 2014, 115, 053710) [6]

a. Does the material studied here show a change of the Seebeck coefficient that could not be explained by a change in the charge carrier concentration? (Could one argue that the energy filtering is observed?)

Answer: Yes. While the Seebeck of the samples studied here are remarkably similar, the carrier concentration and conductivity increase with the addition of (Bi,Sb)2Te3, thus the two are decoupled. We would like to note however this is not the common energy filtering narrative of increasing Seebeck with minimal impact on conductivity.

b. Does this decoupling result in a material with improved maximum power factor or improved electronic portion of the thermoelectric quality factor? (Is this effect beneficial?)

Answer: Only in comparison to their own samples. Optimized Zn_4Sb_3 has a *zT* of 0.8 at 500K[14] which is greater than their best sample at that temperature. Above 500K measurements are unreliable and therefore measurements were not reported above this temperature in (J. Mater. Chem., 2010, 20, 9877 [14]) but the trend continues.

c. Is energy filtering the most likely explanation?

Answer: The paper reports four samples with varying addition of $(Bi,Sb)_2Te_3$ where the properties do not vary monotonously where the range in conductivity is 10%. The 1% sample appears to be an outlier for the trend. The authors do not explain why only the 1% sample show the effect (producing high *zT*). Additionally, this paper does not explain why the carrier concentration of Zn_4Sb_3 increases with addition of $(Bi,Sb)_2Te_3$ in 1% but not 0.5% or 2% sample. β-Zn_4Sb_3 is made of Sb_2^{4-} dimers, Zn^{2+} cations, and Sb^{3-} anions. Bi_2Te_3 electron counting is more simply conceived of with Bi^{3+} cations and Te^{2-} anions. Simple cation for cation or anion for anion substitutions would be Bi_{Zn}^{1+} or Te_{Sb}^{+1},

which are both electron donating defects. Bi_{Sb} would likely be charge neutral, and it is hard to imagine a Te_{Zn} type defect.

The XRD pattern shows$(Bi,Sb)_2Te_3$ as a phase mixed in with β-Zn_4Sb_3. No imaging was done to investigate the morphology of these precipitates to show their size and impact. In order for XRD to detect the relatively sharp $(Bi,Sb)_2Te_3$ peaks the size of this secondary phase would have to be much larger than the nano precipitates predicted to create an energy filtering effect. Why is the carrier concentration is changing definitely deserves further investigation as the papers claims are predicated on the conductivity and carrier concentration change witnessed.

The authors claim that the lowered thermal conductivity is a result from enhanced phonon scattering at grain boundary interfaces but give no reason why the interfacial scattering would be enhanced. Authors claim that the scattering parameter increases with the addition of $(Bi,Sb)_2Te_3$, however the temperature dependence of resistivity is not reflective of this change.

d. Does the paper employ a homogenous or inhomogeneous model for transport?

Answer: The paper employs a homogenous transport model forcing all changes that the samples see in transport into a homogenous scattering parameter. This is done even while the authors talk about the inhomogeneous nature of their samples experiencing higher scattering rates at grain boundary interfaces. The numerous unexplained phenomena witnessed in this study potentially suggests the conventional homogenous model is insufficient for this study.

3 Sb_2Te_3 (Nano Lett. 2011, 11, 2841) [7]

a. Does the material studied here show a change of the Seebeck coefficient that could not be explained by a change in the charge carrier concentration? (Could one argue that the energy filtering is observed?)

   Answer: Yes, the energy filtered sample has a larger carrier concentration and Seebeck coefficient than the non-energy filtered sample.

b. Does this decoupling result in a material with improved maximum power factor or improved electronic portion of the thermoelectric quality factor? (Is this effect beneficial?)

   Answer: No, the power factors between the energy filtered and non-energy filtered sample are the same within error (nanocomposite: 1.02±0.36, Sb_2Te_3: 0.96±0.14 $\mu W/cmK^2$). Additionally, the weighted mobility (electronic portion of the thermoelectric quality factor) of the energy filtered sample goes down from 11.82 to 6.88 cm^2/Vs.

c. Is energy filtering the most likely explanation?

   Answer: No. From the XRD in this paper there appears to be some texturing difference between their samples. The authors did not measure their samples in different orientations to see the effects of anisotropy. Because of this we can't be sure that the changes we see are not from an anisotropy effect commonly seen in these layered materials.

d. Does the paper employ a homogenous or inhomogeneous model for transport?

   Answer: The paper uses a homogenous transport model, even though 9% of their sample by mass is composed of platinum.

4 PbTe (Phys. Rev. B 2004, 70, 115334) [9]

a. Does the material studied here show a change of the Seebeck coefficient that could not be explained by a change in the charge carrier concentration? (Could one argue that the energy filtering is observed?)

   Answer: Yes, generally the nano-grained samples have larger effective masses than the bulk samples, but this paper only compares 3 large grained samples to 17 nano-grained ones.

b. Does this decoupling result in a material with improved maximum power factor or improved electronic portion of the thermoelectric quality factor? (Is this effect beneficial?)

   Answer: No, the power factor of the bulk samples is far superior to the power factor of the nanostructured ones.

c. Is energy filtering the most likely explanation?

   Answer: Yes. The authors present a self-consistent homogenous model that has no major flaws in their logic. Potentially the heterogenous model we propose could explain the phenomena they observe. Because the authors don't measure the thermal conductivity of their samples we can not test this hypothesis. It is definitely worthy of further investigation.

d. Does the paper employ a homogenous or inhomogeneous model for transport?

   Answer: This paper employs a homogenous transport model for all of its analysis despite acknowledging that grain boundary scattering is likely.

5 Ti(Co,Fe)Sb (Acta Mater. 2013, 61, 2087) [10]

a. Does the material studied here show a change of the Seebeck coefficient that could not be explained by a change in the charge carrier concentration? (Could one argue that the energy filtering is observed?)

   Answer: From the included data, yes. However, from the relationship between Seebeck and carrier concentration (Fig. 3d), one can tell that the effective mass m_e^* changes randomly against the InSb concentration.

b. Does this decoupling result in a material with improved maximum power factor or improved electronic portion of the thermoelectric quality factor? (Is this effect beneficial?)

   Answer: Only from the included data, but these materials are in fact worse than other Half Heuslers with similar TiCoSb based composition (i.e. J. Appl. Phys 2007, 102, 103705 [15]).

c. Is energy filtering the most likely explanation?

   Answer: The authors claimed high-mobility electron injection effect, energy-filtering effect, and boundary-scattering effect. From the paper it is very difficult to separate all the effects claimed and make a solid conclusion about their presence. There isn't a clear trend in any of the transport parameters studied in this paper and therefore it's hard to infer much from this data. The effect is clearly much more complicated than energy filtering alone.

   Based on the fact that their control sample deviates significantly from what is found elsewhere in the literature, there are likely variables at play in the authors paper that are not considered.

d. Does the paper employ a homogenous or inhomogeneous model for transport?

Answer: Authors compare their data to a homogenous model to show that the standard homogenous transport model does not fit their data. They leave the question open as to why the standard homogenous model does not fit, but imply it is related to the scattering parameter and not that their sample is inhomogeneous.

6 PbTe (J. Appl. Phys. 2010, 108, 064322) [11]

a. Does the material studied here show a change of the Seebeck coefficient that could not be explained by a change in the charge carrier concentration? (Could one argue that the energy filtering is observed?)

   Answer: No. The low temperature behavior is exactly what would be expected from a shift in carrier concentration. The increasing conductivity with temperature in the best sample is unexpected, however Ag is known to be an amphoteric dopant in PbTe. Ag^{+} substituting for Pb^{2+} is an acceptor while interstitial Ag^{+} is an electron donor. At the high temperatures measured it has been shown that Ag and Cu dissolves and reprecipitates into PbTe changing the charge carrier concentration[16], known as dynamic doping[17]. It is possible that the amphoteric behavior maintains the Fermi Level in the band gap region for high Seebeck coefficient while introducing more charge carriers (both n and p-type) explaining the increase in conductivity with temperature.

b. Does this decoupling result in a material with improved maximum power factor or improved electronic portion of the thermoelectric quality factor? (Is this effect beneficial?)

   Answer: N/A. Decoupling effect is not observed.

c. Is energy filtering the most likely explanation?

Answer: No, See discussion of dynamic doping above. This paper also mentions the nano-composited sample's temperature dependent conductivity is indicative of ionized impurity scattering or grain boundary scattering. What is not answered is how the addition of these scattering mechanisms leads to higher conductivity at higher temperatures when compared to the bulk. This might be due to dopant solubility, but we would need to see temperature dependent hall carrier concentration to verify.

d. Does the paper employ a homogenous or inhomogeneous model for transport?

Answer: This paper employs a homogenous model when analyzing transport, even though it states oxygen at the grain boundaries are crucial to explain the activated conductivity and energy filtering behavior. This paper only measured thermal conductivity and hall carrier concentration at room temperature. The thermal conductivity of the nano-composited sample is noticeably lower than that of the bulk samples. If we had the temperature dependent transport data for these samples, we suspect a two-phase model with an interfacial Seebeck term would quantitively explain the phenomenon these authors witness.

7 $Bi_{85}Sb_{15}$ Graphene Composite (J. Appl. Phys. 2016, 55, 045802) [12]

a. Does the material studied here show a change of the Seebeck coefficient that could not be explained by a change in the charge carrier concentration? (Could one argue that the energy filtering is observed?)

Answer: No. The transport in this paper doesn't follow a trend with graphene content. The Seebeck, conductivity, and carrier concentration are however

roughly in line with one another. As the carrier concentration changes from one sample to another the conductivity and Seebeck also change accordingly.

b. Does this decoupling result in a material with improved maximum power factor or improved electronic portion of the thermoelectric quality factor? (Is this effect beneficial?)

   Answer: N/A. The decoupling isn't observed.

c. Is energy filtering the most likely explanation?

   Answer: No, a decoupling of Seebeck and carrier concentration isn't witnessed. Additionally, the magnitude of the Seebeck of all materials studied here decrease with increasing temperature even from the lowest temperature studied of 180K. This means both electrons and holes are present and active in transport. The paper does not mention how bipolar conductivity would be influencing how they analyze their transport.

d. Does the paper employ a homogenous or inhomogeneous model for transport?

   Answer: The paper employs a homogenous model for transport and does not even consider the effects multiple carrier types would have on their analysis.

After a careful review we found not a single paper used a heterogenous model to analyze an energy filtering effect in their material. Additionally, we found none of the papers could reasonably claim energy filtering was definitely present and leading to an improvement of performance in their materials. Of the paper 7 that used graphene to modify their material, they claimed energy filtering might be an effect, however its data did not show a decoupling between the Seebeck coefficient and carrier concentration.

S2: Transport Measurement Comparison

For the purpose of comparing *zT* of other Mg_3Sb_2 based compounds from the literature, we measure the electrical conductivity and Seebeck coefficient of the $Mg_{3.2}Sb_{1.99}Te_{0.01}$ and its nanocomposites with GNP on an ULVAC ZEM3, as shown in Fig. S1.

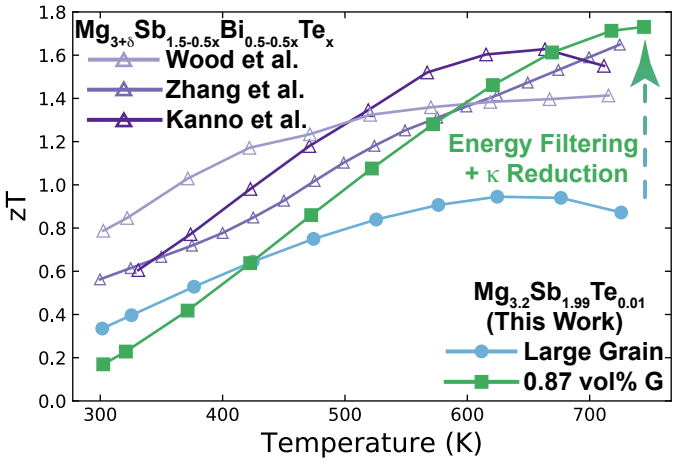

Fig. S1: Temperature dependent *zT* of $Mg_{3.2}Sb_{1.99}Te_{0.01}$ and its nanocomposite with GNP in comparison to state-of-the-art of n-type Mg_3Sb_2 based compounds ($Mg_{3+\delta}Sb_{1.49}Bi_{0.5}Te_{0.01}$) in literature.[18-20] $Mg_{3.2}Sb_{1.99}Te_{0.01}$ has a peak zT of ~0.95 near 650K, which is boost to ~1.73 near 750K with the addition of GNP. This enhancement is a result of increasing the interfacial thermal resistance at grain boundaries with addition of GNP. This increased thermal resistance leads to the synergistic outcomes of reducing the composite's thermal conductivity as well as amplifying the energy filtering effect. The GNP/ $Mg_{3.2}Sb_{1.99}Te_{0.01}$ nanocomposite shows comparable performance over that of $Mg_{3+\delta}Sb_{1.49}Bi_{0.5}Te_{0.01}$ in the temperature range > 600K. In low temperature range, the performance is limited due to grain boundary effect, which results in significant reduction in electrical conductivity. The increase in Seebeck coefficient induced by electron filtering is not large enough to compensate the reduction in electrical conductivity.

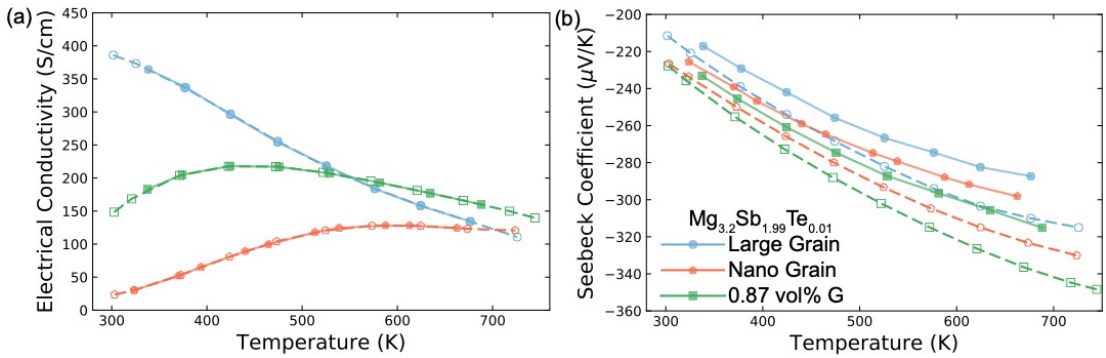

Fig. S2: Electrical conductivity (a) and Seebeck coefficient (b) of $Mg_{3.2}Sb_{1.99}Te_{0.01}$ and its nanocomposite with GNP. Dashed line with unfilled circles represents ZEM-3 measurement. Solid line with filled circles represents measurement from in-house instruments. The conductivity from ZEM-3 shows similar trend as our measured through Van der Pauw measurement, whereas the Seebeck coefficient from ZEM-3 is larger than the measurement setup designed by Iwanaga et al.[21], which may be due to the cold-finger effect.[22]

S3: Development of The Two-Phase Model for A Semiconductor with Grain Boundaries

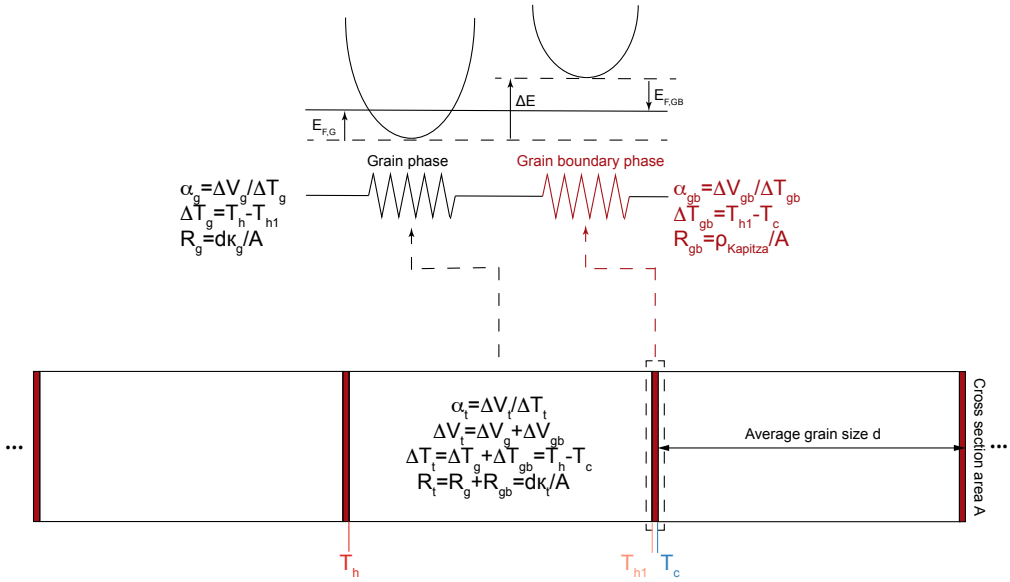

Fig. S3: Illustration of series circuit configuration for a semiconductor with grain boundaries.

S3.1: ΔT_{gb}/ ΔT_t Dependent α_t

For a semiconductor with a given temperature drop ΔT_t, the apparent Seebeck coefficient α_t will be:

$$\alpha_t = \frac{\Delta V_t}{\Delta T_t} \qquad \text{(S1)}$$

The total voltage drop ΔV_t will be a sum of the voltage drop in the grains ΔV_g and the voltage drop at the grain boundaries ΔV_{gb}. Also, the Seebeck coefficient of each phase (α_g for the grains, and α_{gb} for the grain boundaries) will follow the same configuration as Eq. S1. Thus, we have

$$\Delta V_t = \Delta V_g + \Delta V_{gb} = \alpha_g \Delta T_g + \alpha_{gb} \Delta T_{gb} \qquad \text{(S2)}$$

ΔT_t is also the sum of temperature drop in the grains (ΔT_g) and at the grain boundaries (ΔT_{gb}).

$$\Delta T_t = \Delta T_g + \Delta T_{gb} \qquad \text{(S3)}$$

By combing Eq. S1, S2 and S3, one can solve α_t:

$$\alpha_t = \alpha_g + (\alpha_{gb} - \alpha_g)\frac{\Delta T_{gb}}{\Delta T_t} \qquad \text{(S4)}$$

For $|\alpha_{gb}| > |\alpha_g|$ which is the case of electron filtering, a larger fractional temperature drop across the grain boundary regions ($\Delta T_{gb}/\Delta T_t$) will result in a larger total seebeck coefficient (α_t). Thus, in order to achieve maximized α_t, one needs to maximize $\Delta T_{gb}/\Delta T_t$.

The thermal resistance of the semiconductor (R_t) is a sum of thermal resistance in the grain phase (R_g) and thermal interface resistance at the grain boundary (R_{gb}).

$$R_t = R_g + R_{gb} \qquad \text{(S5)}$$

For a semiconductor with average grain size d and cross section area A, one can rewrite Eq. S5 as follows:

$$\frac{d}{\kappa_t A} = \frac{d}{\kappa_g A} + \frac{\rho_{Kapitza}}{A} \qquad \text{(S6)}$$

Here, κ_t and κ_g, are thermal conductivity of the semiconductor and grain phase, and $\rho_{Kapitza}$ is Kapitza resistivity of grain boundary phase.

If we assume thermodynamically stable conditions, with a given constant flow rate (Q') across the semiconductor, we have

$$Q' = \frac{\Delta T_t}{R_t} = \frac{\Delta T_g}{R_g} = \frac{\Delta T_{gb}}{R_{gb}} \qquad \text{(S7)}$$

By combing Eq. S3, S6 and S7, we have

$$\frac{\Delta T_t \kappa_t}{d} = \frac{(\Delta T_t - \Delta T_{gb})\kappa_g}{d} = \frac{\Delta T_{gb}}{\rho_{Kapitza}} \qquad \text{(S8)}$$

By rewriting Eq. S8, we have

$$\frac{\Delta T_{gb}}{\Delta T_t} = \frac{\kappa_t \rho_{Kapitza}}{d} = \frac{1}{\frac{d}{\kappa_g \rho_{Kapitza}} + 1} \qquad \text{(S9)}$$

In order to increase $\Delta T_{gb}/\Delta T_t$, one needs to reduce the grain size d, and/or to increase Kapitza thermal resistivity $\rho_{Kapitza}$. Note that κ_g is the intrinsic property of grain phase, thus will remain the same.

S3.2: How to Solve α_{gb} and $\rho_{Kapitza}$

In a heterogeneous material system with energy filtering effect, the α_t is correlated to its thermal conductivity. By combing Eq. S4, S8 and S9, we have

$$\alpha_t = \alpha_g + \frac{(\alpha_{gb}-\alpha_g)}{\frac{d}{\kappa_g \rho_{Kapitza}}+1} \qquad \text{(S10)}$$

$$= \alpha_g + (\alpha_{gb} - \alpha_g)(1 - \frac{\kappa_t}{\kappa_g}) \qquad \text{(S11)}$$

One is able to solve α_{gb} by rewriting Eq. S11.

$$\alpha_{gb} = \alpha_g + \left(\alpha_t - \alpha_g\right)\frac{\kappa_g}{\kappa_{g-\kappa_t}} \qquad \text{(S12)}$$

In practice, both Seebeck coefficient and thermal conductivity of the semiconductor and grain phase (single crystal) are measurable. Thus, one is able to solve α_{gb} by measuring all these parameters.

Furthermore, one is also able to solve the $\rho_{Kapitza}$ by rewriting Eq. S6.

$$\rho_{Kapitza} = d\left(\frac{1}{\kappa_t} - \frac{1}{\kappa_g}\right) \qquad \text{(S13)}$$

S3.3: Contrasting Result through Reducing d and Increasing $\rho_{Kapitza}$

Under the series circuit configuration, overall thermal conductivity is calculated by (Eq. S6):

$$\kappa_t = \frac{\kappa_g}{1+\frac{\rho_{Kapitza}\kappa_g}{d}} \qquad \text{(S14)}$$

The overall electrical conductivity (σ_t) is under same configuration as the thermal conductivity (Eq. S13), thus we have:

$$\sigma_t = \frac{\sigma_g}{1+\frac{\rho_{el-gb}\sigma_g}{d}} \qquad \text{(S15)}$$

Here, σ_g is electrical conductivity of grain phase. $\rho_{el\text{-}gb}$ is electrical interface resistivity of grain boundary phase.

According to the Wiedenmann-Franz relationship, we have

$$\kappa = \kappa_{electronic} + \kappa_{Lattice} = L\sigma T + \kappa_{Lattice} \qquad \text{(S16)}$$

For grain boundary phase, we have

$$\frac{1}{\rho_{Kapitza}} = L\frac{1}{\rho_{el-gb}}T + \frac{1}{\rho_{Lattice-gb}} \qquad \text{(S17)}$$

Here, $\rho_{Lattice\text{-}gb}$ is the thermal resistivity contribution from lattice at the grain boundary.

$$\rho_{Kapitza} = \frac{1}{\frac{LT}{\rho_{el-gb}}+\frac{1}{\rho_{Lattice-gb}}} \qquad \text{(S18)}$$

Although reducing d can enhance total Seebeck coefficient (Eq. S10), it impairs electrical conductivity simultaneously (Eq. S15), which may result in impairment in power factor. In contrast, increasing $\rho_{Kapitza}$ is an effective approach to minimize the impact to electrical conductivity. One is able to increase the lattice contribution ($\rho_{Lattice\text{-}gb}$) without affecting electronic part significantly (Eq. S18).

S4: Repeatability of Transport Measurements

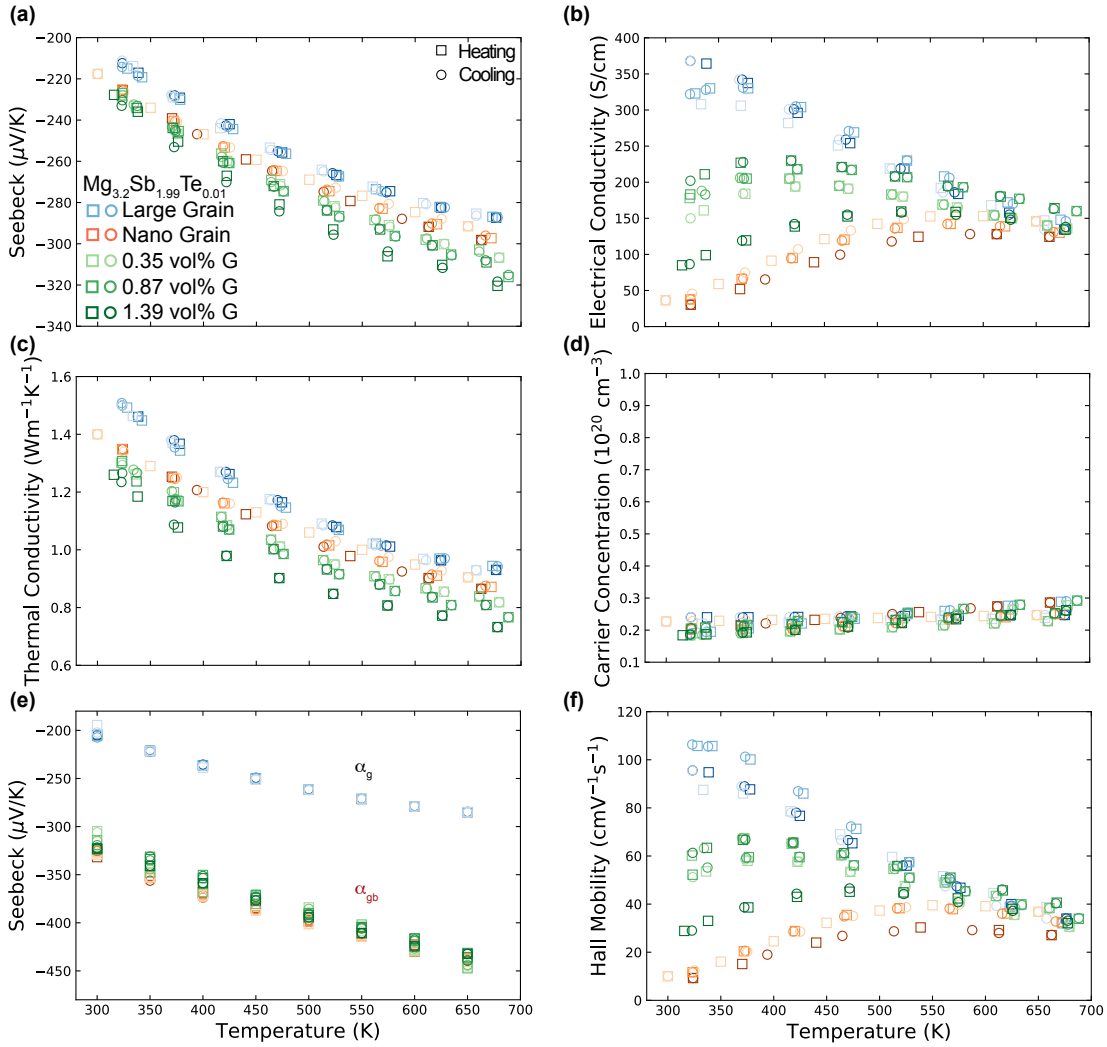

Fig. S4: Seebeck coefficient (a), electrical conductivity (b), thermal conductivity (c), carrier concentration (d) and hall mobility (f) of the $Mg_{3.2}Sb_{1.99}Te_{0.01}$ samples. Blue dots represent three large grain samples, orange dots represent three nano-grained samples, and green dots represents five samples for GNP incorporated nanocomposites (light green for two 0.35 vol% GNP incorporated nanocomposites, medium green for two 0.87 vol% GNP incorporated nanocomposites, and dark green for one 1.39 vol% GNP incorporated nanocomposites). Square dots represent heating cycles, and circle dots represent cooling cycles. All the samples show the same carrier concentration within the measurement error. (e) Calculated Seebeck coefficient of grain phase (α_g) and grain boundary phase (α_{gb}) in the various $Mg_{3.2}Sb_{1.99}Te_{0.01}$ samples with and without the presence of GNP. The different electrical transport performance in various samples is governed by grain boundary effect[19] rather than presence of graphene. The samples with smaller grain size generally exhibit lower electrical conductivity and hall mobility in

the temperature range < 500K. Although carbon nano-materials such as graphene and carbon nanotube owns remarkable electrical transport properties[23], it is worth to point out that the excellent properties may not inevitably result in a consequent improvement in electrical conductivity of inorganic nanocomposites.[24-26]

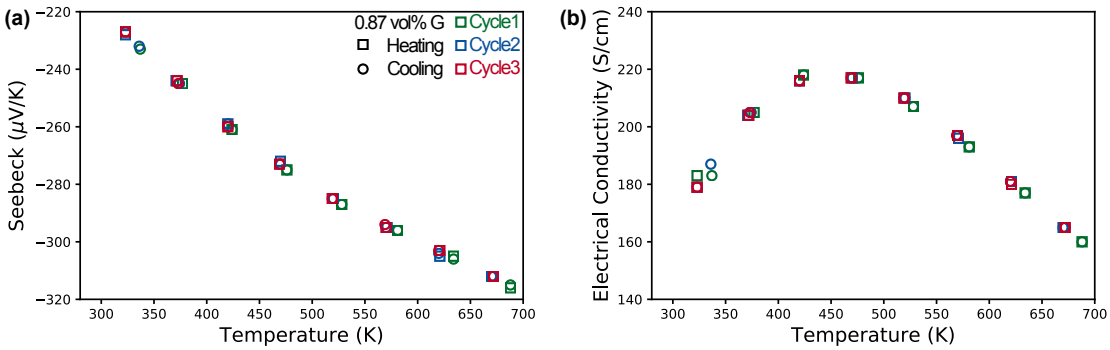

Fig. S5: Seebeck coefficient (a), and electrical conductivity (b) of the $Mg_{3.2}Sb_{1.99}Te_{0.01}$ sample with 0.87 vol% of GNP. The plot shows the cycle stability of the sample with three heating-cooling cycles.

S5: Supporting Figures and Data

S5.1: Correlation between Thermal Conductivity and Seebeck Coefficient

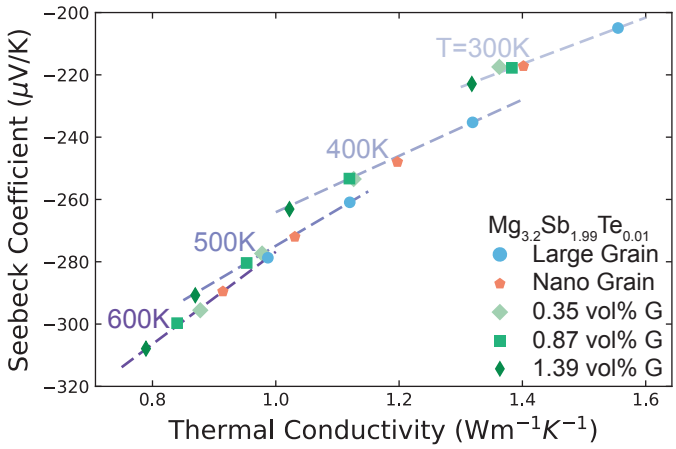

Fig. S6: Correlation between Seebeck coefficient and thermal conductivity. The samples with lower thermal conductivity show larger Seebeck coefficient, signaling the importance of grain boundary kapitza resistance on the energy filtering effect. The purple dashed lines are simulated result by applying Eq. 3 under various temperature. The results confirm linear correlation between Seebeck coefficient and thermal conductivity. All the data points are extracted from the smooth fitted curves in Fig. 3d.

S5.2: Electron Backscatter Diffraction (EBSD)

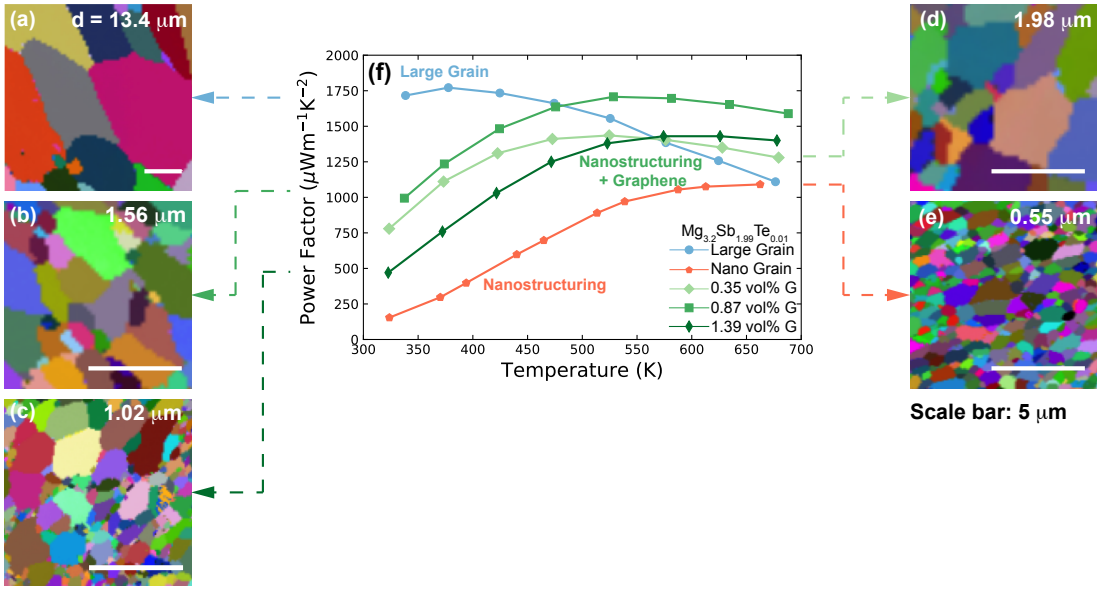

Fig. S7: EBSD maps of the $Mg_{3.2}Sb_{1.99}Te_{0.01}$ samples with and without GNP. (f) Temperature dependent power factor of the samples. (a) to (e) Corresponding EBSD maps of the samples.

S5.3: SEM Microstructure Characterization

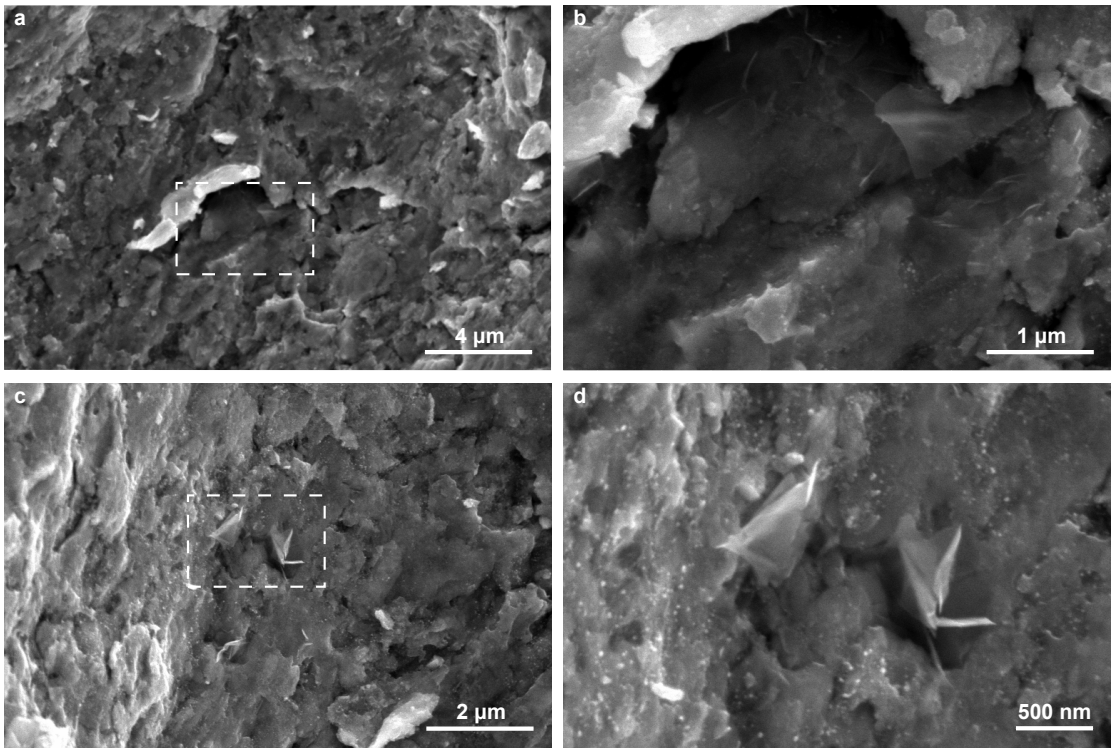

Fig. S8: SEM images of the fracture surface of 0.87vol% G/$Mg_{3.2}Sb_{1.99}Te_{0.01}$ nanocomposite. b & d are the dashed square area marked in a & c in high magnification. The images confirm the presence of GNP nanoplatelets in the nanocomposites without localised aggregation.

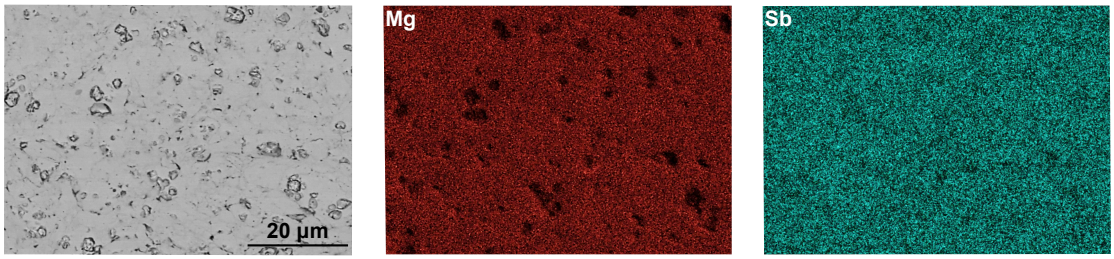

Fig. S9: SEM-EDX (Energy-Dispersive X-ray spectroscopy) maps of polished 0.87vol% G/$Mg_{3.2}Sb_{1.99}Te_{0.01}$ nanocomposite.

S5.4: STEM Analysis

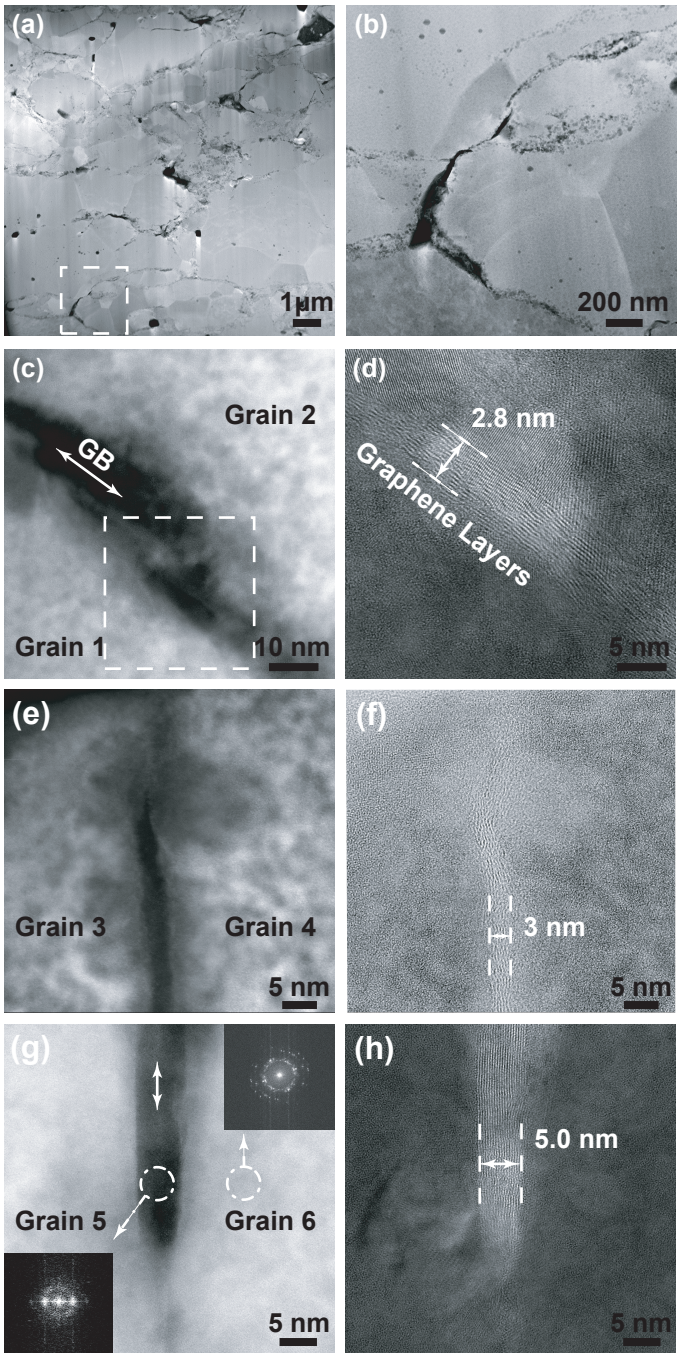

Fig. S10: STEM (scanning transmission electron microscopy) characterization of 0.87vol% G/Mg3.2Sb1.99Te0.01 nanocomposite. (a) & (b) High-angle annular dark-field (HAADF) images of the nanocomposite showing morphology, b is enlarged image of dashed square in a. (c) to (h) grain boundary area filled with GNP nanoplatelets. c, e & g are HAADF images showing grain areas and grain boundary areas. d, f & h are bright field (BF) images showing layer structure of the GNP. The insert images in e are fast Fourier transform (FFT) diffractions of grain area and grain boundary area filled with the GNP.

The FFT of GNP is distinguished with that of Mg3.2Sb1.99Te0.01 matrix. The result suggests an average thickness of ~3 nm for GNP filled grain boundaries.

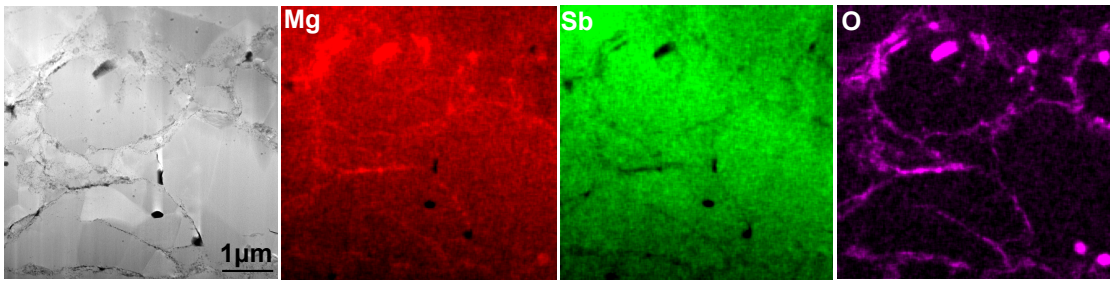

Fig. S11: STEM-EDX maps of 0.87vol% G/$Mg_{3.2}Sb_{1.99}Te_{0.01}$ nanocomposite.

After careful STEM-EDXS analysis of our samples we find MgO is indeed present at the grain boundaries. While this adds further complication to the understanding of what exactly is present at the grain boundaries, the heterogenous transport model we created to analyze our results remains the same. Previous transport models looking at the effect grain boundaries have on Mg_3Sb_2[27] and Mg_2Si[28] have found that some sort of an energy barrier at the grain boundary leads to the increased electrical resistance. The origins of this barrier in Mg_3Sb_2 have been previously rationalized by the existence of Mg vacancies at the boundary[27], whereas de Boor[28] et al. explains the energy barrier in Mg_2Si with the presence of MgO. The exact origin of the grain boundary potential barrier, and its relationship to oxide material definitely deserves further study. The grain boundary structure is likely very complicated involving surface reactions that lead to some MgO, but ultimately this is beyond the scope of this paper. Regardless of its origin, we show this energy barrier region's thermal conductivity can be altered with the addition of GNP therefore revealing Mg_3Sb_2's interfacial Seebeck coefficient.

S5.5: Raman Spectra

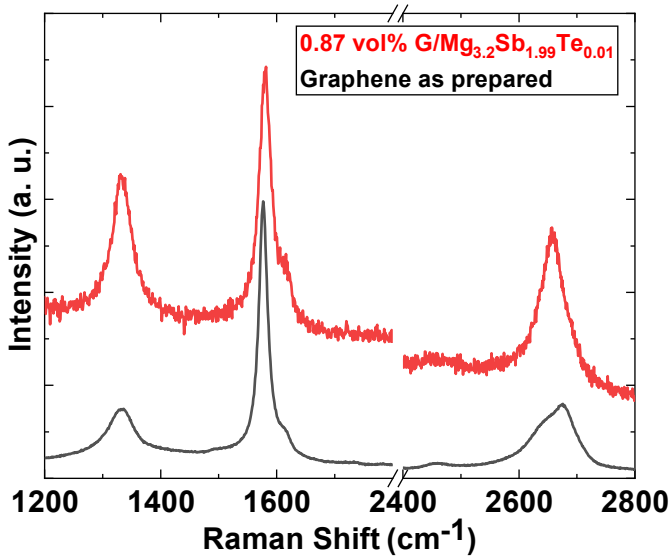

Fig. S12: Raman spectra of GNP nanoplatelets and GNP (G)/$Mg_{3.2}Sb_{1.99}Te_{0.01}$ nanocomposites.

Raman spectroscopy confirms the presence of GNP in the nanocomposites without significant degradation. The D band at ~1340 cm^{-1} is characteristic of disordered or defective carbon structure, such as the edge of graphene. The G band at ~1580 cm^{-1} is characteristic of sp^2 carbon hexagonal networks connected by covalent bonds.[29] The D to G band ratio (I_D/I_G) is a strong indication of defect amounts from the edges of graphene. On the other hand, the full width at half maximum (FWHM) of D peak is a strong indication of defect amount in graphene due to introduction of sp^3 amorphous carbon structure.[30] The I_D/I_G of as prepared GNP in the nanocomposites is ~0.17. In contrast, the I_D/I_G of GNP in sintered nanocomposites increased to ~0.54. Furthermore, the FWHM of D peak (~42 cm^{-1}) is similar for the GNP as prepared and the GNP in the nanocomposites. These observations indicate that the composite processing steps created more defects through creating more edge of GNP (i.e. GNP were broken down into smaller sizes), but did not induce considerable amount of sp^3 defects which significantly destruct the sp^2 carbon hexagonal networks. Furthermore, the 2D peak at

591 ~2660 cm^{-1} is characteristic of the numbers of layer of GNP.[29, 30] The increase in I_{2D}/I_G
592 band together with red shift in peak position indicate that composite processing steps
593 reduced the average layer number of GNP. This observation indicates a uniform
594 distribution of GNP in the nanocomposites without aggregation.
595

S5.6: X-Ray Diffraction (XRD) Patterns

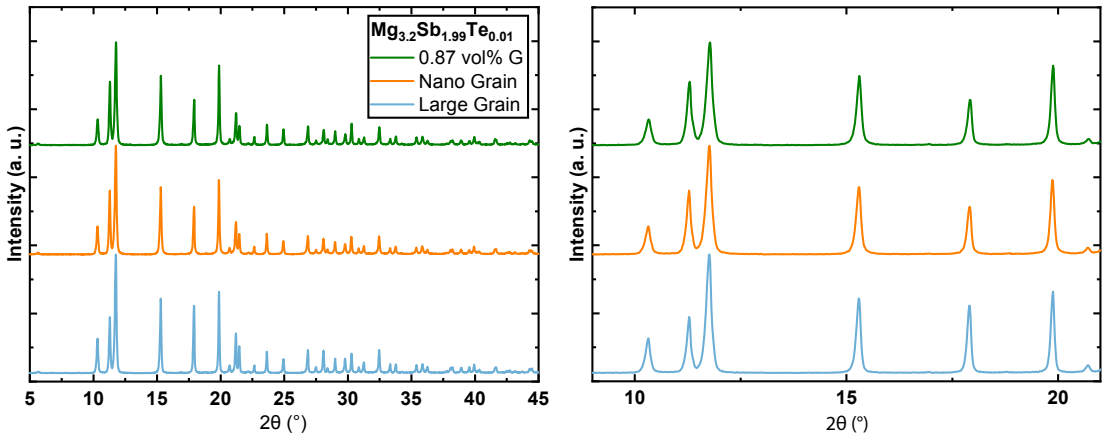

Figure S13: Cu K1α x-ray diffraction in reflection geometry of pelletized samples synthesized for this study. All samples had a nominal composition of $Mg_{3.2}Sb_{1.99}Te_{0.01}$.

X-Ray diffraction on the pelletized samples was carried out on a Stoe STADI-MP in reflection geometry using pure Cu K1α radiation. From XRD there appears to be no detectable impurity phase in any of the samples tested for this study. All peak patterns can be indexed as the Mg3Sb2 (ICSD- 2142) which verifies the formation of the single phase Mg3Sb2 without any impurities or secondary phases.

S5.7: X-Ray Photoelectron Spectroscopy (XPS)

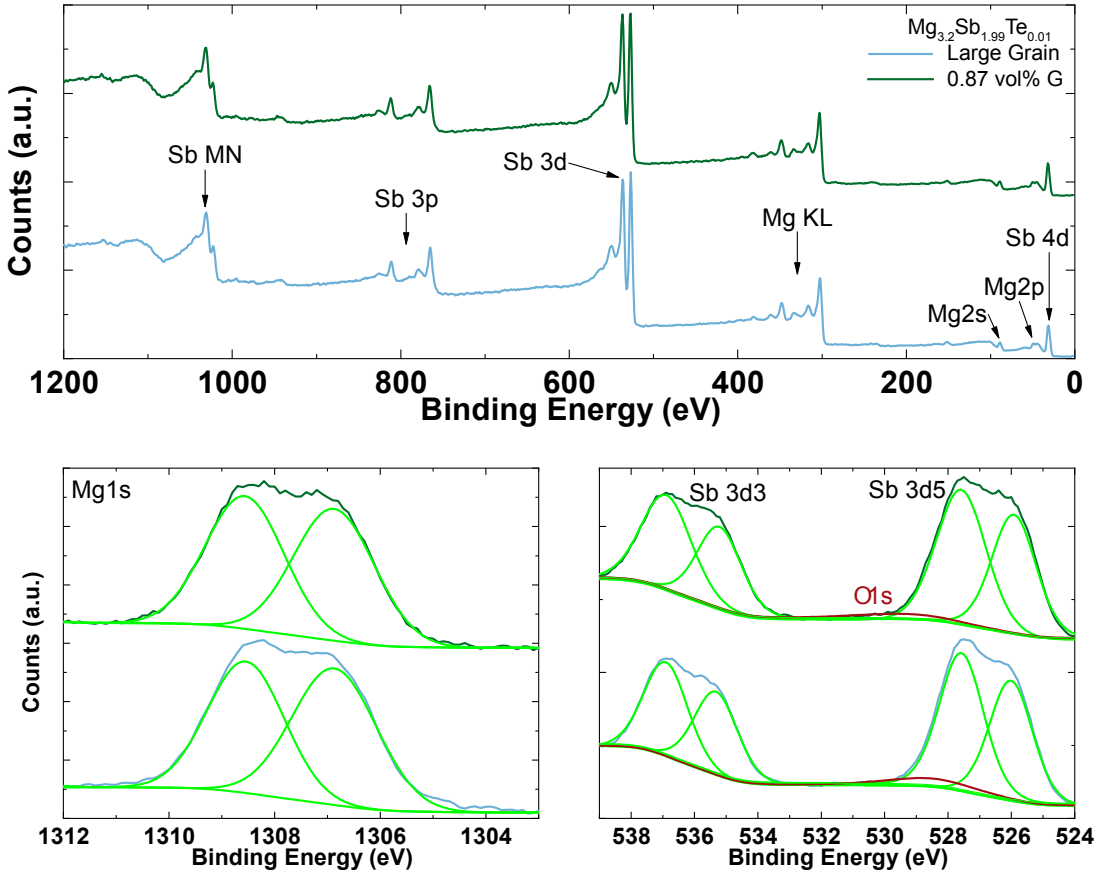

Figure S14: XPS analysis of the $Mg_{3.2}Sb_{1.99}Te_{0.01}$ and its nanocomposites with GNP.

From XPS there appears to be no detectable elemental or compositional change induced by incorporation of GNP. This observation confirms that GNP did not chemically interact with $Mg_{3.2}Sb_{1.99}Te_{0.01}$.

S5.8: Analysis of $Si_{0.80}Ge_{0.20}B_{0.016}$ by Dresselhaus et al.

The two-phase model was applied to analyze $Si_{0.80}Ge_{0.20}B_{0.016}$ literature data reported by Dresselhaus et al.[31]. The $Si_{0.80}Ge_{0.20}B_{0.016}$ samples show strong correlation between Seebeck coefficient and Thermal conductivity after nanostructuring. The data from bulk/advanced SiGe alloy material (P-JIMO, marked as Large grain) were taken to represent the properties of grain phase. The properties of grain boundary phase were then calculated from the nano-grained sample (SGMA04, marked as Nano grain). The analysis indicates a Seebeck coefficient of grain boundary phase to be around 350 μV/K.

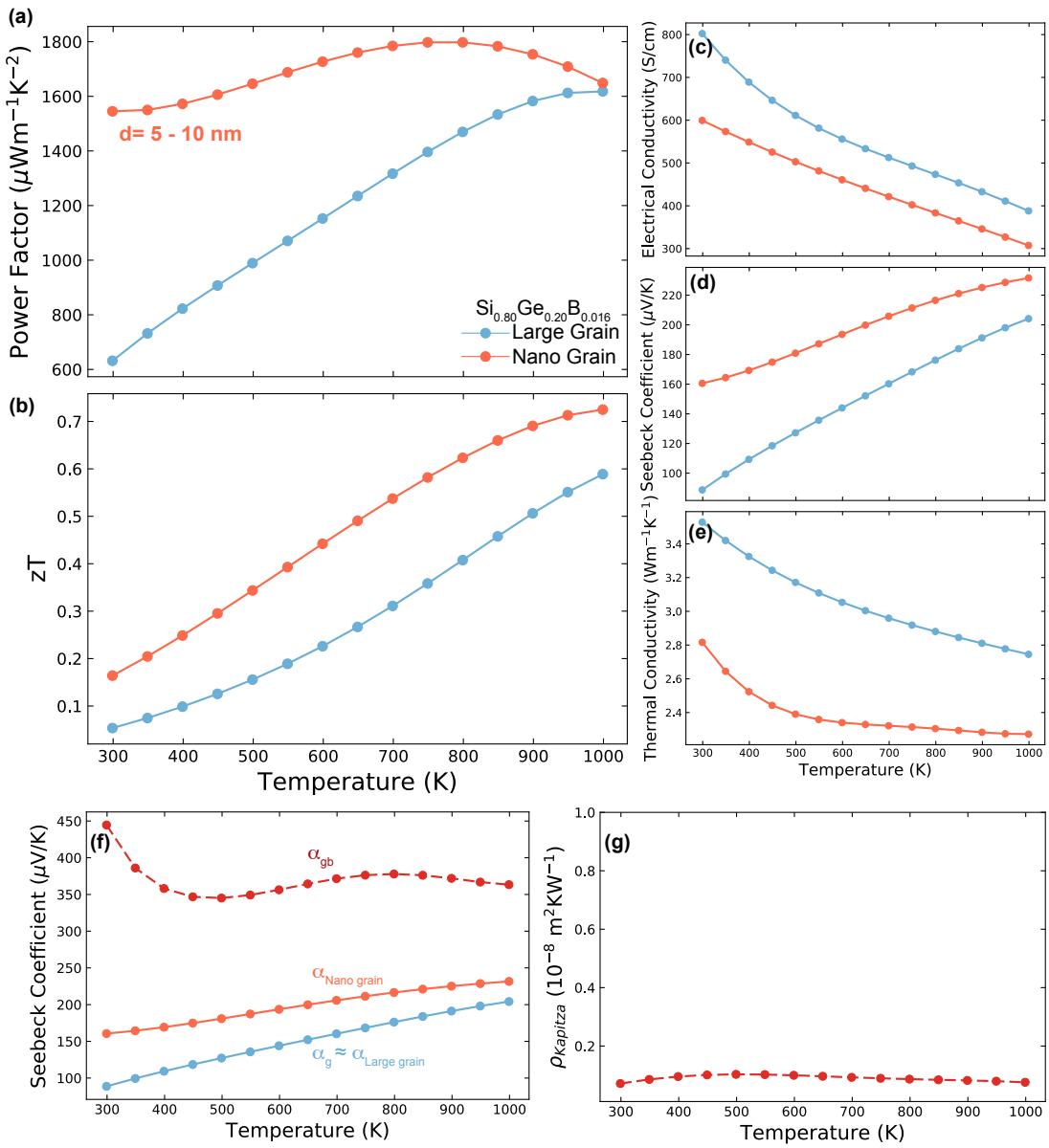

Figure S15: Transport properties of $Si_{0.80}Ge_{0.20}B_{0.016}$ with varying grain size. (a) and (b) Temperature dependent power factor and zT of the samples. (c) to (e) Seebeck coefficient, electrical conductivity and thermal conductivity of the samples. The nano-grained sample exhibit grain boundary effect due to interface scattering.[31] (f) Calculated Seebeck coefficient of grain phase (α_g) and grain boundary phase (α_{gb}). α_{gb} was calculated by applying Eq. 3. α_g was taken from the Seebeck coefficient of the large grain sample. For the large grain sample without the grain boundary effect, the properties are close to those of single crystal with no grain boundaries.[27] (g) Calculated interfacial thermal resistivity ($\rho_{Kapitza}$) of grain boundary phase. $\rho_{Kapitza}$ was calculated by applying Eq. 4. The average grain size is 10 nm as indicated in the literature.

S5.9: Effect of Adding Too Much GNP

For the sample with 1.74 vol% GNP, the measured thermoelectric properties are off the trend. Due to the nature of strong van der Waals interaction, graphene sheets tend to aggregate easily and to form poorly dispersed aggregation. This situation becomes extreme in composite when the GNP concentration reaches a threshold.[32] The aggregation (**Fig. S16**) leads to detrimental effects (**Fig. S17**), including disturbance of electron transport and thermal shorting, observed as a sign of relatively low electrical conductivity, low thermopower (absolute value of Seebeck coefficient), and high thermal conductivity, compared to the other samples. Similar effects were also demonstrated in a few thermoelectric nanocomposites with GNP concentration above a threshold.[24, 33] Although the incorporation of nano-carbon materials to reduce thermal conductivity has also been successfully demonstrated in several thermoelectric materials,[24, 26, 33] aggregation and/ or a continuous interfacial network (percolation) of nano-carbon materials should be avoided, which would severely impair composite performance. Development of novel processing strategy to avoid such aggregation in matrix even at a significant loading is encouraging and may lead to further improvement of thermoelectric performance.

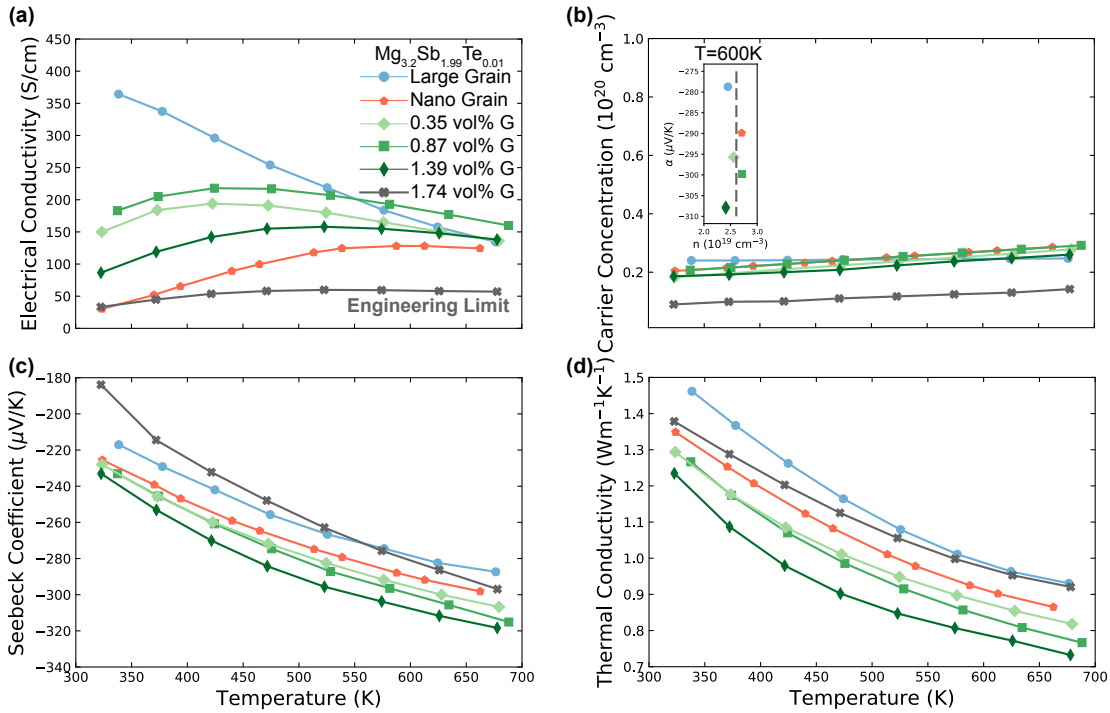

Fig. S16: Transport properties (a to d) of $Mg_{3.2}Sb_{1.99}Te_{0.01}$ with varying GNP concentration. Except for 1.74 vol% G, all other samples exhibit strong correlation between thermal conductivity and Seebeck coefficient (**Fig. 3b** in the main text). The trend agrees with prediction of the applied heterogeneous model (**Fig. 4** in the main text). The addition of GNP did not affect the value of interfacial Seebeck coefficient. By increasing interfacial thermal resistance, the incorporated GNP amplifies the contribution of interfacial Seebeck coefficient, leading to a net increase in bulk Seebeck coefficient. At a certain concentration above 1.39 vol% (i.e. 1.74 vol%), graphene sheets aggregate to form graphite, which severely damages electron transport (a & c), as well as leading to thermal shorting (d). Note here this is a limitation in current processing methodology, rather than break down of the heterogeneous model.

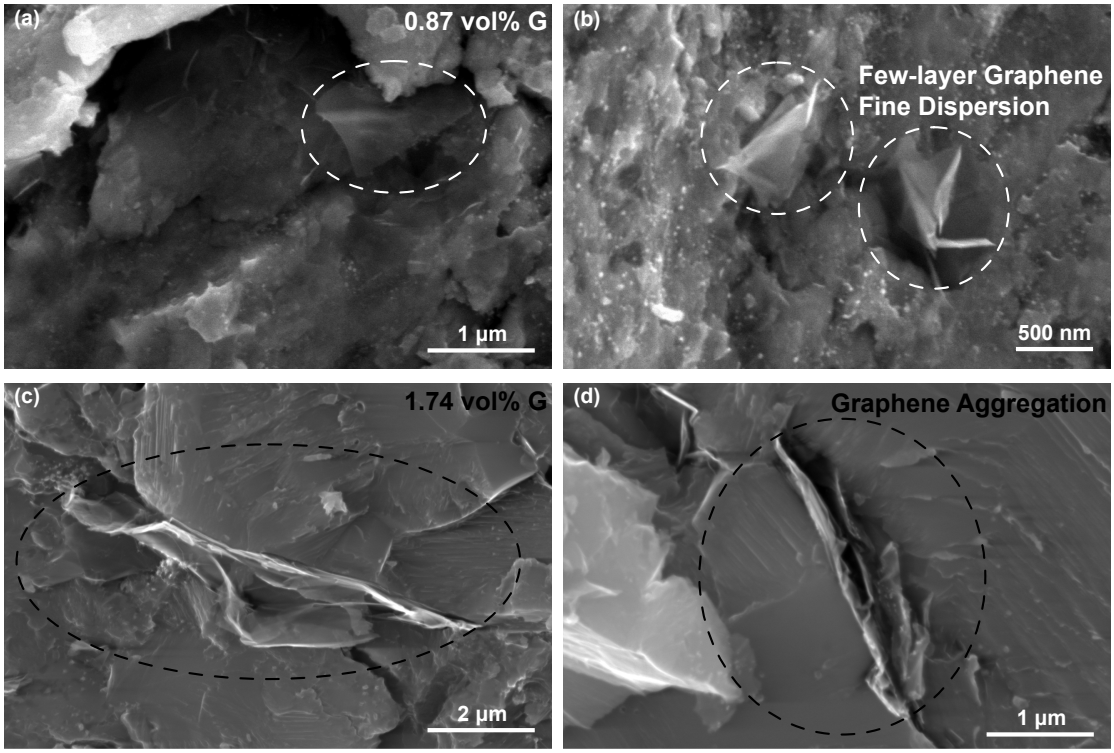

Fig. S17: SEM images of a fracture surface of 0.87vol% G/$Mg_{3.2}Sb_{1.99}Te_{0.01}$ nanocomposite (a & b) and 1.74 vol% G/$Mg_{3.2}Sb_{1.99}Te_{0.01}$. (c & d). Compared with 0.87 vol% G/$Mg_{3.2}Sb_{1.99}Te_{0.01}$ nanocomposite, the graphene sheets severely aggregate to graphite in 1.74 vol% G/$Mg_{3.2}Sb_{1.99}Te_{0.01}$.

S5.10: Grain Size Dependence on GNP Concentration

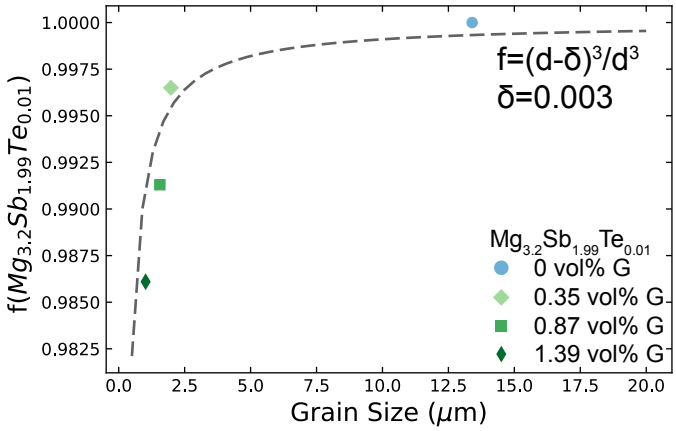

Fig. S17: Grain size dependency on GNP concentration. The grain size decreases with the increasing GNP concentration. The dashed line represents the fitting result of a three-dimensional, two-phase model[34], where f represents the volume fraction of $Mg_{3.2}Sb_{1.99}Te_{0.01}$ grain phase, d is the grain size, and δ is the average thickness of the grain boundary phase. The result indicates an average thickness of 3 nm for grain boundaries filled with GNP, which is consistent with the observation in TEM.

S5.11: Perspective of Energy Filtering Effect in Mg_3Sb_2

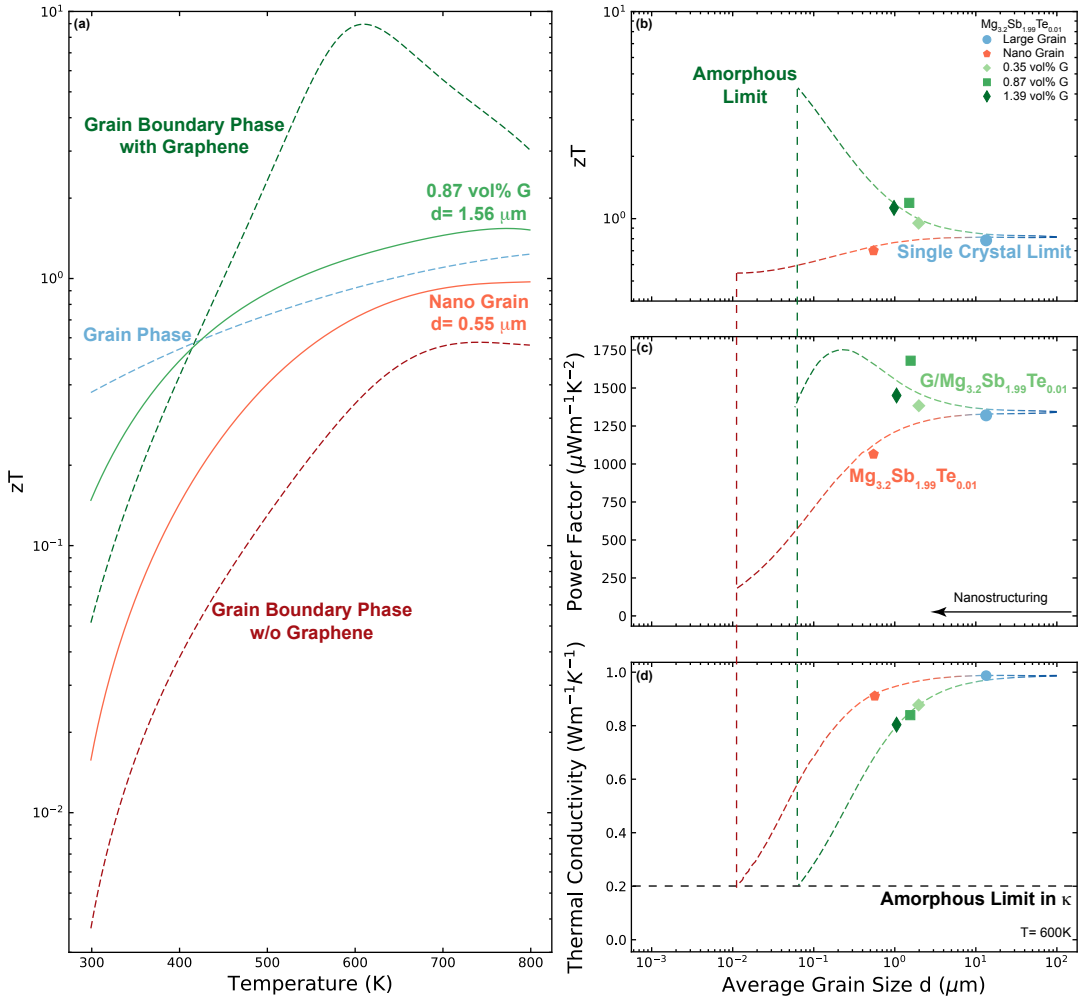

Fig. S18: Thermoelectric performance analysis of Mg_3Sb_2/GNP nanocomposite under the two-phase model. Dashed lines are modelling inferred result, and the solid lines and points are experimental results. (a) zT performance of Mg_3Sb_2 and its nanocomposites follows effective medium theory. The improvement of the total zT in Mg_3Sb_2/GNP nanocomposite is presumably a result of zT_{gb} being greater than the bulk zT consistent with prior analysis of electron filtering.[35]. (b) to (d) Grain size dependence of bulk thermoelectric performance. With an enhanced Kapitza resistance (such as in the case of the nanocomposite), reducing grain size may simultaneously enhance power factor and reduce thermal conductivity, thus improving the bulk zT. Two key factors limiting the bulk thermoelectric performance are Kapitza resistance (affecting both magnitude of power factor and thermal conductivity) and amorphous limit[36, 37] (affecting thermal conductivity). We predict a zT of ~4 at 600 K for Mg_3Sb_2/GNP nanocomposite with grain size of ~60 nm at amorphous limit. Due to aggressive nature of nano-materials, in a composite achieving nano-size grain without aggregation of the nano-materials remains a serve

engineering challenge[32]. In order to achieve such a performance, development of dedicated nano-engineering approaches such as layer-by-layer assembly[38, 39] may be necessary for precise control of nanostructure.

S6: Methods

S6.1: Synthesis of $Mg_{3.2}Sb_{1.99}Te_{0.01}$

Magnesium turing (99.95%, Alfa Aesar), antimony shots (99.9999%, Alfa Aesar), bismuth granules (99.997%, Alfa Aesar), and tellurium lumps (99.999%, Alfa Aesar) were used as starting elements. The nominal composition used for all ball milled samples in this study was $Mg_{3.2}Sb_{1.99}Te_{0.01}$. Stoichiometric amounts of the raw materials were loaded into a stainless steel vial with stainless steel balls. The weight ratio of raw materials to balls is 1:2. The raw materials were mechanically alloyed for 2 hours by using a high-energy mill (SPEX 8000D). The processes were carried out under protection of argon atmosphere. The yielded black powder was collected and stored inside an argon-filled glove box.

S6.2: Preparation of GNP/$Mg_{3.2}Sb_{1.99}Te_{0.01}$ Compound

The GNP were produced by a liquid phase exfoliation method[40]. For production of GNP /$Mg_{3.2}Sb_{1.99}Te_{0.01}$ compound, the calculated amount of GNP and $Mg_{3.2}Sb_{1.99}Te_{0.01}$ powders were dispersed in anhydrous and deoxygenated Dimethylformamide (DMF) with assistance of sonication for 30 minutes. The resultant mixture was then filtered and dried in a vacuum oven for 12 hours under ambient temperature. Before sintering, the compound was mechanically mixed for 5 minutes by using the high-energy mill to ensure uniform distribution of GNP. The weight ratio of raw materials to balls is 1:10 in this case. The processes were carried out under protection of argon atmosphere. For control purpose, the powders for $Mg_{3.2}Sb_{1.99}Te_{0.01}$ samples without GNP were treated with the same process.

S6.3: Sintering and Annealing of $Mg_{3.2}Sb_{1.99}Te_{0.01}$ and GNP/$Mg_{3.2}Sb_{1.99}Te_{0.01}$ Composite

The processed powders were loaded into a graphite die and sintered by using an induction rapid hot press (RHP). For the large grain sample and the samples with GNP, the sintering condition was 1073 K with 45 MPa pressure for 20 minutes. For the nano-grain samples, the sintering condition was 873 K with 45 MPa pressure for 60 minutes. Afterwards, the hot-pressed pellets were annealed at 873 K under a magnesium rich environment for 48 hours.[19] All the processes were carried out under protection of argon atmosphere.

S6.4: Structural Characterization

Microstructures and crystal grain sizes of $Mg_{3.2}Sb_{1.99}Te_{0.01}$ and its nanocomposites with GNP were investigated by scanning electron microscope (Quanta650FEG) equipped with a detector (Oxford Instruments Nordlys). For Chemical analysis, a FEI Quanta 3D scanning electron microscope (SEM) equipped with a field emission gun (FEG) was utilized. Samples were cut and ground down to P4000 SiC paper followed by polishing using 1 μm diamond paste and OPS colloidal silica (20 min polishing time/step) on a Buehler Microcloth, After the polishing steps, the samples rinsed in distilled water, agitated and cleaned in an ethanol-filled ultrasonic bath, blow-dried and then stored over a desiccant. The following SEM operational conditions were employed: accelerating voltage of 10–15 kV and 10 mm working distance. Chemical analysis was carried out using a $10mm^2$ Silicon Drift Detector (SDD) with ultra-thin window (UTW) and TEAM X-ray analysis system.

The analytical scanning transmission electron microscopy (STEM) investigation was

performed using a FEI Tecnai G2 F20 S-TWIN operating at an accelerating voltage of 200 kV, which was equipped with a Bruker XFlash 6130T Silicon Drift Detector (SDD) EDX detector. All data acquisition and post-processing were carried out in FEI TEM Imaging and Analysis (TIA) software and Esprit Software. STEM micrographs were captured using the bright field (BF) and high-angle annular dark-field (HAADF) detectors. For sample preparation, thin foil specimens for subsequent high-resolution microscopy were fabricated via the in-situ lift-out method in a FEI Quanta 3D Dual Beam focused ion beam/scanning electron microscope (FIB/SEM) instruments equipped with OmniProbe micromanipulators. Thin cross-sectional specimens were extracted from the samples using the micromanipulator and then welded onto a copper grid for further ion milling. Prior to milling a layer of Pt was deposited on the region of interest in order to provide protection against ion beam damage on the sample during the lift-out procedure. Subsequently, specimens were lifted out from the sample and transferred onto a copper grid using the micromanipulator and milled down to electron transparency (~100 nm). Lower accelerating voltages, *i.e.* 5 kV and 2 kV with ion current of 48 pA and 27 pA were used in the final thinning process.

Raman spectra were obtained using a Horiba LabRAM HR Evolution Raman spectrometer with an excitation wavelength of 633 nm.

X-ray diffraction measurements were conducted at room temperature on a STOE-STADIMP powder diffractometer with an asymmetrically curved Germanium monochromator (MoKα1 radiation, $\lambda = 0.70930$ Å). The line focused X-ray tube was operated at 50 kV and 40 mA. The sample was placed on a metallic holder and measured in reflection geometry in a rotating stage.

X-ray photoelectron spectroscopy (XPS) measurements were performed using a high vacuum Thermo Scientific ESCALAB 250 Xi XPS system at a base pressure of ~1×10-9 Torr. The XPS data had a binding energy resolution of ~0.1 eV using a monochromated Al Kα X-ray source at ~1486.7 eV (~400 μm spot size). All core-level spectra were the average of five scans taken a dwell time of 50 ms and a pass energy of 50 eV. Samples were charge compensated using a flood gun, and all core-level spectra were charge corrected to adventitious carbon at ~284.8 eV. Sputtering was done in situ using the ESCALAB 250 Xi+ sputtering system with a 3 keV Ar+ ion gun at high current. all subpeaks were determined using the software suite Avantage (Thermo Scientific).

S6.5: Characterization of Electrical and Thermal Transport Properties

The electrical conductivity and Hall coefficient measurements were performed using a 4-point probe Van der Pauw methodology with a 0.8 T magnetic field under high vacuum.[22] The Seebeck coefficients of the samples were determined using chromel-Nb thermocouples by applying a temperature gradient across the sample to oscillate between ±5 K.[21] Thermal conductivity was calculated from the relation $\kappa = DdC_p$, where D is the thermal diffusivity measured with a Netzsch LFA 457 laser flash apparatus, d is the geometrical density of the material, and C_p is the heat capacity at constant pressure. C_p of the compounds were calculated via the polynomial equation proposed by Agne et al.[41] For the purpose of comparison, the electrical conductivity (σ) and Seebeck coefficient (α) were determined simultaneously (under a helium atmosphere) using a ULVAC-RIKO ZEM-3 system. ZEM data was used to compare zT of the samples and previously reported values from literature.

Reference

1. M. Zebarjadi, K. Esfarjani, M. S. Dresselhaus, Z. F. Ren and G. Chen, *Energ Environ Sci*, 2012, **5**, 5147-5162.
2. L. Yang, Z. G. Chen, M. S. Dargusch and J. Zou, *Adv Energy Mater*, 2018, **8**, 1701797.
3. C. Gayner and Y. Amouyal, *Adv Funct Mater*, 2020, **30**, 1901789.
4. L. D. Hicks and M. S. Dresselhaus, *Phys Rev B*, 1993, **47**, 16631-16634.
5. L. W. Whitlow and T. Hirano, *J Appl Phys*, 1995, **78**, 5460-5466.
6. T. H. Zou, X. Y. Qin, D. Li, B. J. Ren, G. L. Sun, Y. C. Dou, Y. Y. Li, L. L. Li, J. Zhang and H. X. Xin, *J Appl Phys*, 2014, **115**, 053710.
7. D.-K. Ko, Y. Kang and C. B. Murray, *Nano Lett*, 2011, **11**, 2841-2844.
8. A. Soni, Y. Q. Shen, M. Yin, Y. Y. Zhao, L. G. Yu, X. Hu, Z. L. Dong, K. A. Khor, M. S. Dresselhaus and Q. H. Xiong, *Nano Lett*, 2012, **12**, 4305-4310.
9. J. P. Heremans, C. M. Thrush and D. T. Morelli, *Phys Rev B*, 2004, **70**, 115334.
10. W. J. Xie, Y. G. Yan, S. Zhu, M. Zhou, S. Populoh, K. Galazka, S. J. Poon, A. Weidenkaff, J. He, X. F. Tang and T. M. Tritt, *Acta Mater*, 2013, **61**, 2087-2094.
11. B. Paul, V. A. Kumar and P. Banerji, *J Appl Phys*, 2010, **108**, 064322.
12. M. S. El-Asfoury, M. N. A. Nasr, K. Nakamura and A. Abdel-Moneim, *Jpn J Appl Phys*, 2016, **55**, 045802.
13. A. Bhardwaj, A. K. Shukla, S. R. Dhakate and D. K. Misra, *Rsc Adv*, 2015, **5**, 11058-11070.
14. E. S. Toberer, P. Rauwel, S. Gariel, J. Tafto and G. J. Snyder, *J Mater Chem*, 2010, **20**, 9877-9885.
15. T. Wu, W. Jiang, X. O. Li, Y. F. Zhou and L. D. Chen, *J Appl Phys*, 2007, **102**, 103705.
16. Y. Z. Pei, A. F. May and G. J. Snyder, *Adv Energy Mater*, 2011, **1**, 291-296.
17. L. You, J. Y. Zhang, S. S. Pan, Y. Jiang, K. Wang, J. Yang, Y. Z. Pei, Q. Zhu, M. T. Agne, G. J. Snyder, Z. F. Ren, W. Q. Zhang and J. Luo, *Energ Environ Sci*, 2019, **12**, 3089-3098.
18. T. Kanno, H. Tamaki, H. K. Sato, S. D. Kang, S. Ohno, K. Imasato, J. J. Kuo, G. J. Snyder and Y. Miyazaki, *Appl Phys Lett*, 2018, **112**, 033903.
19. M. Wood, J. J. Kuo, K. Imasato and G. J. Snyder, *Adv Mater*, 2019, **31**, 1902337.
20. J. W. Zhang, L. R. Song, S. H. Pedersen, H. Yin, L. T. Hung and B. B. Iversen, *Nat Commun*, 2017, **8**, 13901.
21. S. Iwanaga, E. S. Toberer, A. LaLonde and G. J. Snyder, *Rev Sci Instrum*, 2011, **82**, 063905.
22. K. A. Borup, J. de Boor, H. Wang, F. Drymiotis, F. Gascoin, X. Shi, L. D. Chen, M. I. Fedorov, E. Muller, B. B. Iversena and G. J. Snyder, *Energ Environ Sci*, 2015, **8**, 423-435.
23. A. K. Geim and K. S. Novoselov, *Nat Mater*, 2007, **6**, 183-191.
24. P. A. Zong, R. Hanus, M. Dylla, Y. S. Tang, J. C. Liao, Q. H. Zhang, G. J. Snyder and L. D. Chen, *Energ Environ Sci*, 2017, **10**, 183-191.
25. P.-a. Zong, J. Liang, P. Zhang, C. Wan, Y. Wang and K. Koumoto, *Acs Appl Energ Mater*, 2020, **3**, 2224-2239.

26. R. Nunna, P. F. Qiu, M. J. Yin, H. Y. Chen, R. Hanus, Q. F. Song, T. S. Zhang, M. Y. Chou, M. T. Agne, J. Q. He, G. J. Snyder, X. Shi and L. D. Chen, *Energ Environ Sci*, 2017, **10**, 1928-1935.
27. J. J. Kuo, S. D. Kang, K. Imasato, H. Tamaki, S. Ohno, T. Kanno and G. J. Snyder, *Energ Environ Sci*, 2018, **11**, 429-434.
28. J. de Boor, T. Dasgupta, H. Kolb, C. Compere, K. Kelm and E. Mueller, *Acta Mater*, 2014, **77**, 68-75.
29. L. M. Malard, M. A. Pimenta, G. Dresselhaus and M. S. Dresselhaus, *Phys Rep*, 2009, **473**, 51-87.
30. J. B. Wu, M. L. Lin, X. Cong, H. N. Liu and P. H. Tan, *Chem Soc Rev*, 2018, **47**, 1822-1873.
31. M. S. Dresselhaus, G. Chen, M. Y. Tang, R. G. Yang, H. Lee, D. Z. Wang, Z. F. Ren, J. P. Fleurial and P. Gogna, *Adv Mater*, 2007, **19**, 1043-1053.
32. I. A. Kinloch, J. Suhr, J. Lou, R. J. Young and P. M. Ajayan, *Science*, 2018, **362**, 547-553.
33. Y. Lin, C. Norman, D. Srivastava, F. Azough, L. Wang, M. Robbins, K. Simpson, R. Freer and I. A. Kinloch, *Acs Appl Mater Inter*, 2015, **7**, 15898-15908.
34. J. E. Carsley, J. Ning, W. W. Milligan, S. A. Hackney and E. C. Aifantis, *Nanostruct Mater*, 1995, **5**, 441-448.
35. C. B. Vining and G. D. Mahan, *J Appl Phys*, 1999, **86**, 6852-6853.
36. G. Pernot, M. Stoffel, I. Savic, F. Pezzoli, P. Chen, G. Savelli, A. Jacquot, J. Schumann, U. Denker, I. Monch, C. Deneke, O. G. Schmidt, J. M. Rampnoux, S. Wang, M. Plissonnier, A. Rastelli, S. Dilhaire and N. Mingo, *Nat Mater*, 2010, **9**, 491-495.
37. C. Chiritescu, D. G. Cahill, N. Nguyen, D. Johnson, A. Bodapati, P. Keblinski and P. Zschack, *Science*, 2007, **315**, 351-353.
38. K. Kang, K. H. Lee, Y. M. Han, H. Gao, S. E. Xie, D. A. Muller and J. Park, *Nature*, 2017, **550**, 229-233.
39. A. K. Geim and I. V. Grigorieva, *Nature*, 2013, **499**, 419-425.
40. Y. Lin, J. Jin, O. Kusmartsevab and M. Song, *J Phys Chem C*, 2013, **117**, 17237-17244.
41. M. T. Agne, K. Imasato, S. Anand, K. Lee, S. K. Bux, A. Zevalkink, A. J. E. Rettie, D. Y. Chung, M. G. Kanatzidis and G. J. Snyder, *Mater Today Phys*, 2018, **6**, 83-88.